7-2019

Engineered Porous Media for Groundwater Contaminant Remediation: Applications of Nano-TiO2

Sheng Yin
The University of Texas Rio Grande Valley

ENGINEERED POROUS MEDIA FOR GROUNDWATER CONTAMINANT REMEDIATION: APPLICATIONS OF NANO-TiO_2

A Thesis

by

SHENG YIN

Submitted to the Graduate College of
The University of Texas Rio Grande Valley
In partial fulfillment of the requirements for the degree of

MASTER OF SCIENCE

July 2019

Major Subject:Agricultural, Environmental, and Sustainability Sciences

ENGINEERED POROUS MEDIA FOR GROUNDWATER CONTAMINANT REMEDIATION: APPLICATIONS OF NANO-TiO_2

A Thesis
by
SHENG YIN

COMMITTEE MEMBERS

Dr. Chu-Lin Cheng
Chair of Committee

Dr. Yuanbing Mao
Committee Member

Dr. Jason Parsons
Committee Member

Dr. James Jihoon Kang
Committee Member

Dr. Jongmin Kim
Committee Member

July 2019

ABSTRACT

Sheng, Yin, Engineered Porous Media For Groundwater Contaminant Remediation: Applications Of Nano-TiO_2. Master of Science (MS), July, 2019, 55 pp., 8 tables, 13 figures, 65 references, 18 titles.

Nonmetallic arsenic and hydrocarbon BTEX are the most harmful contaminants commonly found in groundwater. Many oxide, biological and metal based adsorbent materials have been investigated in the laboratory and in the field environment. These materials, especially nano-TiO_2, have been extensively studied in laboratory due to its high efficiency and remediation outcomes. Two forms of synthetic nano-TiO_2, aggregated dendritic nano-scale anatase TiO_2 and polymorphed rutile nano-TiO_2 attached to the surface of SiO_2, were compared to study the feasibility of nano-TiO_2 in geo-environmental engineering applications. Characterization of crystal structure, purity/mixture, and morphologic, microscopic features of the materials were examined by XRD, XRF and SEM, respectively. The arsenic and BTEX removal rate/efficiency were compared between the two materials. The tested nano-TiO_2 were found efficient in mixing ratio and can be potentially scalable in field applications for multiple contaminants.

ACKNOWLEDGMENTS

First and foremost, I am grateful for joint graduate support from UTRGV School of Earth, Environmental and Marine Sciences (SEEMS, College of Sciences) and Industrial Assessment Center funded by DOE-EERE for energy, water and waste management (Department of Civil Engineering, College of Engineering and Computer Science) over the two year period. In addition, I thank UTRGV College of Sciences for awarding me with Science Technology and Engineering Partnership for Success (STEPS) Endowment. Secondly, I especially would like to show my deepest gratitude to my advisor, Dr. Chu-Lin Cheng, who has provided me with support and valuable guidance in every stage of the writing of this thesis. I also thank to the committee members, Dr. Yuanbing Mao, Dr. Jason Parsons of Department of Chemistry, Dr. James Jihoon Kang of SEEMS, and Dr. Jongmin Kim of Department of Civil Engineering, to provide lab and equipment support, as well as the needed knowledge in relevant fields and patience to my questions. Last but not least, I thank Dr. James Hinthorne, Mr. Tom Eubanks and few peer graduate students, who had helped, guided, accompanied me along the journey.

TABLE OF CONTENTS

Page

LIST OF TABLES

Page

LIST OF FIGURES

Page

CHAPTER I

INTRODUCTION

Importance of water and scarcity can't be over-stated in the increasing influence of climate change. Freshwater resources, which only accounts for less than 3% of the total water sources of the earth, support ecosystem health and many human activities in urban and rural areas (Gleick, 1993). However, many countries and regions around the world are facing a lack of clean water supplies and a series of health related issues that followed (Oki and Kanae, 2006). According to the latest United Nation report, approximately half the global population are already living in potential water shortage areas, while the corresponding number of the population is still increasing (UNESCO, 2018).

In order to help mitigate this issue, related technologies and management methods are constantly being proposed, such as seawater desalination, use of groundwater, and wastewater treatment. In contrast, groundwater is more affordable in its sustainability usage, management, and technical research (Aeschbach-Hertig and Gleeson, 2012). During the treatment of groundwater, As and benzene, toluene, ethylbenzene and xylene (BTEX), have received more attention for various reasons, including their high toxicity, carcinogenicity, and environmental hazards of pollutants. Many adsorption-based materials, including and not limited to activated

carbon, organic polymer materials, and metals and their oxides, have been synthesized and improved in the laboratory for such contaminants. Although some of these materials have been used in engineering sites, still many materials that lack an assessment of the potential of the relevant engineering.

The goal of this project is to engineer an efficient and cost-effective nano porous material that can remove As and BTEX in groundwater, and also be suitable for in-situ application at remediation sites. Research objectives are to: (1) investigate characteristics, forms, structures of two types of lab-engineered synthetic Nano-TiO_2; and (2) examine their efficiency in removing As and BTEX. The lab-scale flow column experiment setup is designed to simulate field in-situ applications such as permeable reactive barrier (PRB).

CHAPTER II

REVIEW OF LITERATURE

As in Groundwater

With the widespread use of groundwater, some environmental and health issues have been concerned. Arsenic (As), is one of the most anxious pollutants in groundwater not only because it is indiscernible, tasteless, and odorless, but also due to its natural presence and widespread distribution in groundwater in many parts of the world. It moves into groundwater through natural processes and a range of biological and human activities, including agricultural activities, weathering processes and volcanic eruptions (Nordstrom, 2002; Smedley and Kinniburgh, 2002). As a result of acute and chronic exposure to high levels of As, human in the danger of the adverse health effects, such as gastrointestinal symptoms caused by arsenic, even genotoxicity, mutagenesis, and carcinogenesis (NRC, 1997). Therefore, arsenic has been pointed out by the World Health Organization (WHO) and United States Environmental Protection Agency (US EPA) as the most serious inorganic contaminants in drinking water, specifically, the maximum contaminant level (MCL) of arsenic in drinking water is 10 ug/L in the US (US EPA, 2001), which is same as stated by the WHO guidelines (WHO, 1998).

Multitudinous technologies have been utilized in the treatment of arsenic-containing

water. Table 1 shows some of the commonly used measurement technologies for arsenic in groundwater in the laboratory and on site. Based on factors such as cost, operability and stability, subsurface barriers and solidification are more suitable for use in current practical projects without significantly reducing the removal efficiency (Evanko and Dzombak, 1997; Mulligan, et al., 2001).

To begin with, alum as well as iron (and iron salt), by the processes of coagulation and filtration, is diffusely used to remove the arsenic from water (Kartinen and Martin, 1995). Moreover, anion exchange and reverse osmosis techniques can be used to remove arsenic from water. Similarly, filtration adsorption of adsorbent media is also a potential technology to be used, while many related adsorbent materials, such as biochemical materials, chemical synthetic materials, and metals and their oxides or inorganic compounds, have been proposed by researchers (Mohan and Pittman, 2007; Gupta and Chen, 1978; Hering, et al., 1996; Kim, et al., 2004). For metals and their inorganic solid compounds are used as adsorbents, such as activated alumina, iron, iron hydroxide, iron oxide, and titanium dioxide (TiO_2), have been evaluated their effectiveness about removing arsenic by numerous studies (Kanel, et al., 2005; Pierce and Moore, 1982; Katsoyiannis and Zouboulis, 2002; Kim, et al., 2004; Pena, et al., 2005). Among these adsorbents, TiO_2, especially nano-TiO_2, have an outstanding effect of removing arsenic at pH=6.5-8.5, which is as well as the natural water pH range (Bang, et al., 2011).

Due to the potential of nano-TiO_2 in removing arsenic from water, in the laboratory, the research, including the influencing factors of adsorption, on the removal of arsenic in water by

nano-TiO_2 has also achieved some progress. First of all, the size of TiO_2 and the pH value can affect on As(V) and As(III) adsorption and As(III) photo-oxidation(Pena, et al., 2005; Pena, et al., 2006; Xu and Meng, 2009). In detail, the TiO_2 was effective for As(V) removal at pH=8 while the maximum removal for As(III) is when pH at approximate 7.5 in wastewater (Pena, et al., 2005). As for the size of the nano-TiO_2, Nano-anatase TiO_2, for arsenic removal, is the most efficient, especially the size of 6.6nm. Additionally, the other characters of the material itself, such as TiO_2 content, degree of crystallization, nano-TiO_2 arrangement, has a certain effect on the results of the adsorption (Bang, et al., 2005; Jegadeesan, et al., 2010). However, contact time for adsorption is also indispensable, in the laboratory, the common adsorption time is generally from 30mins to 24h (Pena, et al., 2005; Guan, et al., 2012). Factors such as temperature, pressure, and liquid flow rate all have an effect on the adsorption of TiO_2 (Adamson and Gast, 1967).. The target in this study is groundwater, and these factors more stable in groundwater (Fitts,2002).

BTEX in Groundwater

With the rapid development of the complex industry, a large number of volatile organic compounds (VOCs) were produced, which compounds migrate to soil and groundwater and contaminates them. The BETX, one type of VOCs, which refers to compounds benzene, toluene, ethylbenzene, and xylene, is another pollutant of concerns (Zytner, 1994; Paixão, et al., 2007). The BTEX is mainly derived from human activities, including the wildly use of petroleum and related products, exhausted automobile exhaust, burnt coal and biomass, the usage of paint and leakage from the petrochemical industry (Zalel and Broday, 2008). BTEX would transport with

water and inevitably affect human activities and production, such as drinking water, agricultural water and industrial water. BTEX has different levels of harm to human health. For instance, benzene and ethylbenzene are classified as carcinogens and potential carcinogens, respectively, while toluene and xylene are classified as non-carcinogens (WHO, 1998). Therefore, the USEPA regulates MCL of BTEX in drinking water, which is shown in Table. 2.

In order to remove the BETX from the natural water and drinking water, a series of potential and novel researches and methods were proposed. One of the studies is the use of biological materials or microbial materials, such as the biosorption and degradation of large biomass, including algae and special bacteria (Crawford R, and Crawford D, 2005; Costa, et al., 2012; Ciesielczuk, et al., 2019; Khodaei, et al., 2017). Although biosorption has been used in the treatment of sewage, whether it can be used in in-situ groundwater treatment still requires long-term observation because of its strict requirements on the adsorption environment, and potential ecological pollution (Crini and Lichtfouse, 2018; Hlihor, et al., 2017; Reinhard, et al., 2005). On the other hand, non-biosorbent materials have also made notable advancement. The modified zeolite and different active carbon have made good progress in removing BETX (Ranck, et al., 2005; Lu, et al., 2008; Su, et al. 2010). In addition, metal-based materials and nanotechnology, such as calcium, iron, zinc, and titanium, also have great potential for catalytic degradation (Xue, et al., 2018; Aziz and Kim, 2017; Bharatvaj, et al., 2018). There are few important studies in BTEX removal. For example, it was found that the mixing conditions of nitrate and sulphate can accelerate the natural attenuation of BTEX (Cunningham et al., 2001; Schreiber and Bah, 2002). However, in the prior technology, metals and their oxides, specially

TiO_2, are operable in the treatment of groundwater.

In term of the applications of TiO_2, it is commonly used as a photocatalyst, which has low-toxicity, durability, photocatalytic activity and stability at pH range 6.5-8.5 (Alizadeh Fard, et al., 2013; Han, et al., 2009). Alizadeh Fard et al. (2013) studied the effects of the factor including pH, reaction time, hydrogen peroxide concentration and some related ions. Moreover, TiO_2-based composites are also being used for BTEX removal, with many materials with removal efficiencies exceeding 90% or even about 99%. (Alizadeh Fard, et al., 2013; Li, et al., 2005; Li, et al., 2009; Peerakiatkhajorn, et al., 2012; Zou, et al., 2006).

For this research, the form in which groundwater is in contact with the catalyst or adsorbent material in field is applied to provide the feasibility of two different forms nano-TiO_2 to remove the As and BTEX for field applications. XRF was used for elemental composition analysis, while the XRD was carried out for crystal structure information, and surface morphology were characterized with SEM. The removal efficiency of two materials for As and BTEX was collected, under different flow rate (or contact time), and different initial pollutant concentrations.

CHAPTER III

METHODOLOGY AND FINDINGS

Materials and Methods

Materials

All chemicals used were the analytical grade, while all solutions are prepared with deionized (DI) water. As stock solutions were prepared from sodium arsenate dibasic heptahydrate ($Na_2HAsO_4 \cdot 7H_2O$) (Sigma-Aldrich Science, St. Louis, MO, USA) dissolved in DI water, and the BTEX-contaminated water. In addition, the chemicals for preparing nano-TiO_2 include hydrogen peroxide (H_2O_2) (Fisher Scientific, Fair Lawn, NJ, USA), sodium hydroxide solution (NaOH) (Fisher Scientific, Fair Lawn, NJ, USA), SiO_2, titanium chloride ($TiCl_3$) (Fisher Scientific, Fair Lawn, NJ, USA), and 2.0M hydrochloric acid (HCl) (Fisher Scientific, Fair Lawn, NJ, USA). However, the pH was adjusted within a reasonable range of 6.5-8.5 by adding 0.1M NaOH, and 0.1M HCl during the experiment.

20.9 mg of $Na_2HAsO_4 \cdot 7H_2O$ is weighed and dissolve in DI water, and 50 mg/L of As(V) solution is prepared using a 100 ml volumetric flask. Subsequently, 3 ml and 12 ml of the solution are taken out, and approximate 0.15 mg/L and 0.60 mg/L As(V) solution are respectively prepared using a 1000 ml volumetric flask. Finally, the exact concentrations were

determined with an inductively coupled plasma-optical emission spectrometry (ICP-OES, Thermo Jarrell Ash, the U.S.), which has a working range from ppb to ppm concentrations, after each experiment.

Gasoline saturated water is prepared by mixing 90 mL of gasoline, which bought from a local gas station, and 900 mL DI water in a 1 L glass bottle and stirring continuously for 48 hours with a magnetic stirrer (Mao, et al., 2010). Two 10 ml saturated solutions were taken twice and the concentrations (total BTEX) were diluted to 4.5 ppm and 10 ppm, respectively. For the experiment, two sets of 480ml of the same solution were taken, and then added 20ml of H_2O_2 and DI water respectively. The extract concentration was determined with Sitelab UVF-3100 (Sitelab Corporation, Massachusetts, USA) after the experiment for total BTEX.

Two different forms of nano-TiO_2 were used in this study. The first one is aggregated dendritic nano-scale TiO_2, which was produced by using a modified hydrothermal method in the presence of H_2O_2 and NaOH (Mao, et al., 2006). Another form is polymorphed nano-TiO_2 attached to the surface of SiO_2. In other words, the nano-TiO_2 was uniformly attached (e.g., coating) to nano-SiO_2 by adding 0.166 M $TiCl_3$ in 2.0 M HCl and SiO_2, while simultaneously passing O_2 through the mixture at 100 mL/min (Leal, et al., 2017).

The first material was made by synthetic sodium hydrogen titanate nanostructures (Figure. 1a). 35 mL of a 2.5M NaOH solution and 3 mL of 30% H_2O_2 solution were initially mixed into a 45 mL autoclave, with a 1 × 1 cm^2 titanium foil. Then, the autoclave was sealed and heated for 12 h at 150 °C in order to produce the sodium hydrogen titanate. Subsequently, the prepared

nanomaterials that have been washed were neutralized with 30 ml of 0.1 M HCl. After washing, it was annealed at 450 °C for 10 h to obtain the final nano-TiO_2.

The synthesis of the mixed TiO_2 and SiO_2, shown in Figure. 1b, was repeatedly carried out by adding 0.166 M $TiCl_4$ and 2 - 5g SiO_2 , whose particle diameter was less than 125 μm, to 2.0 N HCl. Subsequently, the sample was continuously stirred at a temperature of 60 °C and O_2 was passed through the mixture at 100 mL/min for about 8 hours. The sample was then naturally cooled to room temperature and centrifuged at 3000 rpm for 5 minutes. Finally, the material was washed several times with deionized water, centrifuged, and oven dried at 700 °C, which converts TiO_2 into rutile form, overnight to the final material.

Material Analysis and Characterization

X-ray fluorescence (XRF), a in-house Bruker XRF Tracer IV-SD (XRF, Bruker, U.S.), was applied to determine the elemental composition of materials. It equipped with Silicon Drift Detector (SDD) technology with a 150 eV resolution. The spectra and data were collected by the BrukerS1 analytical program. Measurements were performed at 40 Kev and 15 microamps, with Pd collimator, and the analysis area is ellipse shape with a area about 4x6 mm.

X-ray powder diffraction (XRD), was performed to obtain crystal structure information about two different dried nano-TiO_2. Diffraction patterns of TiO_2 crystal structures were collected with a Bruker D8 ADVANCE (XRD, Bruker, the U.S.), which setted in Chemistry, X-ray diffraction meter with Cu Ka_1 radiation (l = 1.54Å). Moreover, the XRD data were collected by utilizing a scanning mode of 2θ value, whose ranging from 20^o to 90^o with a scanning step size of 0.005^o and a scanning rate of 1.0^o min^{-1}.

Scanning electron microscope (SEM). was used to observe the mic-morphology of dried nano-TiO_2. using a Sigma VP Carl Zeiss scanning electron microscope (FE-SEM, Zeiss, the German), which was placed in the engineering department, manipulated at 5 kV.

Batch experiments

For arsenic adsorption experiment, it was divided into two parts. The first part is to put two kinds of 2-3g TiO2-based materials into 100ml arsenic solution with a concentration of 0.15 and 0.6 mg/l, sealed and placed in the oscillator for 1h at 150 rpm. And 10 mL aliquot at specific time intervals to determine its adsorption efficiency

The second part was based on the laboratory injection system to study the relationship between injection speed and removal efficiency. Both of arsenic adsorption and BTEX catalytic degradation were conducted under the same system. A schematic diagram of the system used in the lab experiment is shown in Figure. 2. The system is consisted of the Erlenmeyer flask, as storage for contaminated groundwater; and the syringes in the pump are used to collect clean water separately; the switch to control the progress of the experiment; the Pump 11 Elite Infusion/Withdrawal Programmable Dual Syringe (Harvard Apparatus, Cambridge, MA, USA), for regulating the rate of water flow or total water flow, simultaneously control the flow direction; and the column filled with 2g TiO_2 may be made from glass, plexiglass, or other suitable material. The column is packed with the reactive medium in such a way as to ensure a homogeneous matrix (Figure. 2). A small amount of white fine sand and some mesh filter materials are placed at the bottom of the column to prevent nano- or micron scale titanium dioxide from entering the

final clean water with water flow, besides, those sand can also, to some extent, simulate the environment in groundwater, and adjust the permeability of the entire adsorbent material. Furthermore, water was driven in the column from bottom to top throughout the whole experiment, in order to better simulate lower flow rates and to minimize the interference of trapped air in the column. All experiments were performed at least three times and results are presented as averages.

Specifically, Figure. 2a is designed for As removal, while Figure. 2b is designed for BTEX removal. Considering the volatility of BTEX, in Fig 2b, the conical flask was sealed, and the pumping gas was used to flow the BTEX-containing water from bottom to top through the TiO_2. In addition, the UV lights are used to support provide the photocatalytic environment for this experimental design (Figure.2b). Also in BTEX experiment, the polytetrafluoroethylene (PTFE) tubing and H_2O_2 were used to prevent BTEX from being absorbed by tubing and affecting the concentrations during experiment.

Moreover, the parameters of environmental condition in the experiment are shown in Table 3. The temperature and pressure of the whole experiment were held constant at 25°C and 101.325 kPa, respectively. The initial concentrations of As and BTEX were set as 0.15-0.7 and 4.5-10.5 mg/L (ppm) separately. The pH value of the solution was 7 ± 0.5, which is consistent with the pH of fresh water in nature. And the flow rate, which controlled the injected 10 ml of wastewater, was kept between 0.66-10.0 ml/min for As removal, and 0.14-1.0 ml/min for BTEX experiment, in order to make the contaminant better in contact with nano-TiO_2. The quality of

both materials in the two parts of the experiment is 3.5g. The removal efficiency of pollutants at different flow rates and the change of pollutant removal efficiency after repeated TiO_2 at the same flow rate were measured.

TiO_2 regeneration

One of the advantages of TiO_2 as an adsorbent is that it can be regenerated, restored, and reused repeatedly. In this study, aggregated TiO_2 based materials for arsenic removal would be regenerated with strong acids and bases. First, the TiO_2 was immersed in 2M NaOH for one hour, the solid-liquid ratio was about 1:10, and the solid component was continuously washed with DI water to neutrality. Subsequently, TiO_2 was soaked in 2M HCl for one hour, and after centrifugation, the solid was rinsed to neutral for later use. XRF was used to examine the regeneration of the adsorbent. For attached TiO_2, directly washed repeatedly by DI water and dry in order to prevent damage to its structure. In terms of the TiO_2 which removes BTEX, both materials can be directly washed repeatedly by DI water, dried after centrifugation and then put them into use. In addition, XRF was also used for analyzing the regenerated TiO_2 in order to compare the XRF pattern and obtain the purity (i.e., mixture) of materials.

Results and Discussions

Characterization of materials

XRF Analysis. XRF spectrum pattern of two different form nano-TiO_2 is shown in Figure. 3. The analysis before the batch experiments was mainly to detect and confirm the purity of experimental materials, while the XRF analysis after experiments is predominantly to study the

changes in the composition of two different nano-TiO_2 after removing contaminants, and the present form of contaminants on the surface of the material.

In Figure. 3, the red line is aggregated dendritic TiO_2, while the blue curve represents TiO_2 attached to the surface of SiO_2. In both XRF of the aggregated TiO_2 and the attached TiO_2, the two highest peaks are in the interval of the element of Ti when compared to the standard range, and those two distinct peaks are significantly and far higher than the other peaks. This result indicates that the element-purity of the two nao-TiO_2 prepared in our experiments is extremely high. Notably, because the materials tested were at nanoscale. Plastic bags and related holders were used to ensure the proper testing of TiO_2 under XRF. In Figure. 3, the peak, which is far lower than Ti peak is only detected in attached TiO_2 is the interval of the element of Si. While the content of Si was much smaller than the content of Ti in the material. It is the result of the 2 - 5g SiO_2 we added to the reaction solution when we made attached TiO_2. At the same time, it also proves that TiO2 in the material of attached nano-TiO_2 is enough to completely enclose the surface of the nano-SiO_2.

XRD Analysis. Pre-experimental XRD analysis was conducted to collect material surface structure information, including crystal structure, particle size etc., while the post-experimental XRD analysis was directed to check the changes in surface structure of the material in order to analyze potential alterations in material structure and effects on these processes during adsorption and catalytic adsorption.

According to the XRD results, the aggregated TiO_2 (red) is fully crystalline anatase TiO_2. In Figure. 4, the red XRD pattern showed contains the two highest and strong diffraction peaks of 2θ values at 25° and 48°, which the specific values of the peaks are 25.5°, 38.9°, 48.3°, 55.2° and 63.1° respectively. Likewise, the aggregated TiO_2 is hexagonal anatase phase of TiO_2 according to its diffraction peaks. The peaks were in consistent with the standard spectrum (Joint Committee on Powder Diffraction Standards, JCPDS Card No. 21-1272) and few earlier studies (Mao, et al., 2006; Thamaphat et al, 2008). In addition, no peak of rutile or brookite phase was detected in the XRD results of the aggregated TiO_2, indicating high purity of the product structure. In other words, the product of aggregated TiO_2 is almost completely crystallized and forms a high-purity hexagonal anatase nano-TiO_2.

Similarly, as for the XRD result (blue) of nano-TiO_2 attached to the surface of SiO_2, the attached TiO_2 is more inclined to be rutile polymorph (Figure. 4). The major strong diffraction peaks, which at 2θ=27.9°, 36.6°, 54.9°, were displayed in the blue XRD pattern. While the other less intense diffraction peaks are concentrated separately at 2θ values of 41.7° and 57.2°. The positions and intensities of diffraction peaks conform to the standard documents (JCPDS Card No. 21-1276) and expected result as well as aggregated TiO_2. Obviously, the TiO_2 wrapped on the surface of SiO_2 is completely rutile without any anatase phases or brookite phases. This material was prepared at 60°C, which is consistent with previous research results (Leal, et al., 2017).

SEM Characterization. In SEM observations, the specific morphology and preliminary

combination of the two different nano-TiO_2 were observed from Figure. 5 (a) the aggregated dendritic TiO_2, (b) the TiO_2 attached to the surface of SiO_2. In terms of morphology, the anatase-type TiO_2 surface has a dense dendritic feelers (Figure. 5a), because it is purposeful in the process of making sodium titanate to have a high specific surface area, which can well contact with water. The SEM characterization of the intermediate product, sodium titanate, which is shown in Figure. 6. The prepared aggregated sodium titanate already has a dendritic initial structure. Specifically, the surface of the sodium titanate (Figure. 6) has numerous tentacles that extend outward, and which has no dendrites like the subsequent TiO_2. However, the main characteristics of TiO_2 formed by neutralization and high-temperature annealing of sodium titanate remain unchanged (Figure. 5a). As for attached TiO_2 (Figure. 5b), It was observed that there were many spherical and hemispherical protrusions, whose size ranges from 50nm to 2μm, on the surface of the material, those protrusions increased the specific surface area of the material, making the contact area of the material with the water flow larger in subsequent experiments. Moreover, there are many nano-scale small protrusions on the main part of the larger protrusions and materials, which make the surface of the material not smooth, and even make the surface of the material appear uneven. This is an alternative to increase the specific surface area of the attached TiO_2.

In terms of combination, both materials are micron-sized particles that are aggregated by nano-TiO_2 (Figure. 5). More combination details can be described by SEM images of different sizes. Figure. 7 and Figure. 8 are aggregated TiO_2 and attached TiO_2, respectively, at different

magnifications SEM observations. In Figure. 7, due to the presence of numerous dendritic tentacles, these micron-sized spherical material component particles, which aggregated by anatase nano-TiO_2, are present in many hollows, which allows the combined materials to have high porosity and permeability. While in Figure. 8, the rutile nano-TiO_2, which attached to SiO_2, exhibits irregular angular crystal micron-sized particles, compared with the hollow nature of aggregated TiO_2, the attached TiO_2 is more closely bonded to each other, and the material particles themselves do not have too much porosity, therefore, the permeability can be controlled according to the macroscopic combination of the material particles in subsequent lab experiments.

Contaminant removal

Arsenic adsorption curve. In this part, a small amount of TiO_2 material is mixed with a large amount of the arsenic solution and stirred to obtain an adsorption curve. The concentration of arsenic solution prepared for the experiment was determined by ICP-OES to be 634ppb (Figure. 9. Group a) and 167ppb (Figure. 9. Group b), respectively, and the adsorption efficiency curve of different Arsenic concentrations is shown in Figure. 9 and Table. 5. In Figure. 9. the two red curves mean the adsorption efficiency of aggregated dendritic TiO_2 in different concentrations of the arsenic solution, while two blue curves are the representative of TiO_2 attached to the surface of SiO_2.

By comparing the curves, the anatase-based TiO_2 material aggregated obviously has better removal efficiency (Figure 9). Also during the one hour of sampling, the Rutile-based attached

TiO_2 has higher adsorption speed in the initial stage of adsorption and can reach the equilibrium of adsorption faster. Moreover, for both of two TiO_2 materials, the higher the substrate concentration of the arsenic solution, the higher the adsorption efficiency of TiO_2. The standard error of the first ten minutes was large, but not more than 10%. The entire mixing system did not reach an equilibrium state at the beginning of the experiments, resulting in a certain deviation of the sample. In the subsequent time, the mixed system operation begun to stabilize, and the standard error of the samples do not exceed 2% (Table 5).

On the one hand, when the low-concentration arsenic-containing wastewater far exceeds the adsorbent material, the adsorption effects of the two materials are similar, while the adsorption rate of the attached TiO_2 is faster. On the other hand, for high concentration (Figure. 9. Group a), the adsorption rate of attached TiO_2 is slightly higher than that of aggregated TiO_2, but the overall adsorption effect of aggregated TiO_2 is a little better than that of attached TiO_2.

Arsenic removal rate. In the second part of arsenic removal is based on the laboratory injection system. In each experiment, 10 ml of the arsenic solution flows through the collected TiO_2, so that arsenic in a small volume of solution can be better removed. This part is to simulate and get the result of the best arsenic removal effect on site. Their result is shown in Figure. 10. and Table 6. Analogously, the red and blue curves aggregated dendritic TiO_2 and TiO_2 attached to the surface of SiO_2, respectively. In Figure. 10. the same arsenic solution, whose different initial concentration of are (a) 634ppb and (b) 167ppb, is also used.

The arsenic is more fully removed when a small amount of solution flows over the

aggregated material. For aggregated TiO_2, the removal efficiencies are 96% (Figure. 10a) and 82% (Figure. 10a) for the two concentrations of the arsenic solution, respectively. While the attached TiO_2 is 92% and 81%. Through the error analysis, the standard error of the arsenic removal rate obtained by the two materials is less than 4% (Table 6).

Furthermore, similar to the Arsenic adsorption curve, in the 15mins of the experiment, aggregated TiO_2 has better removal rate, although the attached TiO_2 has higher adsorption efficiency in the initial stage. Also, the substrate concentration of the arsenic solution is positively correlated with the removal rate.

Overall,the process of adsorption of arsenic by TiO_2 is basically consistent with the first-order kinetics:

$$\ln(arsenic\ \ removal\ \ rate) = -k \cdot t \tag{1}$$

The above two sets of experiments show that both TiO_2 materials have the potential to be used in engineering for arsenic removal. Both materials may have similar removal efficiencies during the initial stages of arsenic removal. After that, due to the slightly faster adsorption rate of the attached TiO_2, the attached TiO_2 will first reach the adsorption saturation, but in general, the aggregated TiO_2 will have better arsenic removal efficiency.

Total BTEX degradation. The total BTEX degradation efficiencies for TiO_2 catalysis and H_2O_2 concentration are tested in the UV system to evaluate the catalytic effects of the two materials (Figure. 11; Table 7). In Figure. 11 (a) and (b) respectively aggregated TiO_2 and attached TiO_2 in three different environments, which including only UV lighting (black),

TiO_2+UV lighting (red), and TiO_2+UV lighting+H_2O_2 (blue).

In Figure. 11. C_0 is the initial concentration of BTEX, which is tested as 4.25 ppm, C is the BTEX concentration in collected solution after different injection times. By comparing the case of only the UV lighting environment, the decomposition of BTEX is very dilatory. However, the adding of TiO_2 alone or with H_2O_2 significantly alter the decomposition rate of BTEX over a period of time. The standard error of the catalytic effect of aggregated TiO_2 is not more than 3%, the standard error of while attached TiO_2 is almost no more than 5%, except for a point of about 10% at 40mins (Table. 7).

Moreover, the higher concentration was used, which measured as 10.17 ppm, also to compare the removal efficiencies for total BTEX (Figure. 12; Table 8). In Figure. 12. the red curve is aggregated dendritic TiO_2, while the blue curve means TiO_2 attached to the surface of SiO_2. The removal efficiency without any TiO_2 is 96.5% in 70 mins. For aggregated TiO_2, the removal efficiency is 21%, and it is 32% for attached TiO_2. The standard error of the catalytic effect (Table 8) of two TiO_2-based is not more than 3%.

All BTEX degradation processes are consistent with first-order kinetics:

$$\ln(\frac{C_t}{C_0}) = -k \cdot t \tag{2}$$

Where the C_t is the concentration of As (M), C_0 is the initial concentration of As (M) and k is the first-order rate constant for species degradation (min^{-1}).

Specifically, in the case of UV/TiO_2 system (no added H_2O_2), the decomposition efficiency of BTEX for the two materials in 70mins is 87% (a) and 75% (b). While the

efficiencies significantly change to 95% (a) and 91% (b) when the H_2O_2 is added to the system. For the systems without H_2O_2, the catalytic efficiency of aggregated TiO_2 is significantly better than that of attached TiO_2 (Figure. 11 and 12), but after adding H_2O_2, the catalytic efficiency of the two materials is not much different (Figure. 11). For the two forms of TiO_2, the rutile is a stable crystal form with the good crystal structure, fewer crystal defects, and fewer oxygen vacancies, while the anatase has more oxygen vacancies, which can capture electrons and increase the separation time of electron holes. Thus, anatase has a better photocatalytic effect (Anpo and Kamat, 2010). In this experiment, aggregated TiO_2 is mainly anatase, and attached TiO_2 is mainly rutile, so the former in the experiment is obviously superior to the latter in the photocatalytic effect on BTEX.

Regeneration of materials.

The XRF pattern of the regenerated TiO_2, which treated arsenic and BTEX separately, is compared with the pre-experiment XRF. Figure. 13 shows (a) the XRF of the aggregated dendritic TiO_2, and (b) the XRF of TiO_2 attached to the surface of SiO_2. The green line represents the XRF pattern of the material before the experiment, while the red and blue curves are respectively the XRF pattern of regenerated TiO_2 after arsenic and BTEX treated. The regeneration of both of the materials is excellent.

In Figure. 13a., the XRF diagram for regenerate dendritic TiO_2, which removes BTEX, the composition of the elements is not much different from the composition of the TiO_2 element before the experiment. Differently, as for TiO_2 for removing arsenic, a small amount of arsenic

remains on the surface of TiO_2 after regeneration. In addition, there are very few increases in chlorine in the material, probably because the use of HCl in the arsenic solution for pH adjustment or during regeneration leads to more chloride, which is not fully removed by DI water.

In terms of the XRF of attached TiO_2, analogously, after adsorption of arsenic, chloride and arsenic elements, which have not appeared before the experiment, are detected in the regenerated TiO_2 powder. Especially, during the regeneration process, there is a small decrease in silicon content, probably because it is consumed in the reaction of acid and alkali, or it may be because the initial silicon content of the sampled powder material is different.

Through the comparison before and after the regeneration experiment, the two TiO_2 materials can be recycled repeatedly, so the conclusion can be concluded that TiO_2 has outstanding engineering application potential due to the good recyclability of the material.

CHAPTER IV

SUMMARY AND CONCLUSION

The two nano-TiO_2 materials have different characterizations, forms, and arrangement, as shown in Table 4. The aggregated TiO_2, which is anatase form, is consistent with not only the standard spectrum of JCPDS Card No. 21-1272, but also the previous studies (Mao et al., 2006; Thamaphat et al., 2008). While the attached nano-TiO_2, which is a polygon rutile, form conformed with the spectrum by JCPDS Card No. 21-1276.

In terms of characterizations of produced nano-materials, there are many dendritic tentacles on the aggregated TiO_2 surface, and the particles are tightly bound together with many hollow and voids of different sizes. As for attached nano-TiO_2, it has the rugged surface and those surface has many spherical and hemispherical bulges. The aggregated material particles are tightly connected and do not have large voids or hollow.

In terms of the effectiveness of the adsorption of arsenic and the catalytic decomposition of BTEX, both TiO_2-based materials demonstrate outstanding capabilities. For arsenic removal, aggregated dendritic TiO_2 has a larger capacity in As adsorption, while the attached TiO_2 has a faster adsorption rate for arsenic removal. It indicates that the attached TiO_2 has advantages for higher flow rates of arsenic-containing wastewater treatment. The dendritic TiO_2 is main based

on anatase, while the attached TiO_2 is mainly formed by rutile.

The results of anatase form having better arsenic adsorption than rutile is consistent with previous studies (Ma and Tu, 2011; Bang, et al., 2005). Another possible explanation is that with the same mass of materials, the attached TiO_2 has less TiO_2 mass due to the presence of added SiO_2, hence lesser adsorption than the actual unit mass of TiO_2.

For BTEX degradation, aggregated dendritic TiO_2 has more significant advantages, due to more oxygen vacancies, anatase can capture electrons and increase the separation time of electron holes. Therefore, anatase has better photocatalysis (Anpo and Kamat, 2010; Su et al., 2011). Moreover, the photocatalytic effect of the attached TiO_2 is better than that of the individual rutile in the literature. This is because the presence of SiO_2 enhances the photocatalytic activity, thereby improving the degradation of BTEX by the material (Zou, et al., 2006; Anderson and Bard, 1997). In short, considering the respective advantages of the materials, including the reuse of materials, and the good removal effect for BTEX and As, both materials tested have great potential in engineering application

CHAPTER V

LIMITATIONS AND FUTURE WORK

Few potential limitations might need to be considered in future work. First, although the cost of synthetic production is relatively lower in the laboratory, the cost of TiO_2 is higher than other materials on the market. In addition, there are energy input requirements, such as high temperature during material production and the needs of continuous UV exposure during operation for hydrocarbon remediation. Water hardness can also be an important factor as magnesium and calcium ions would affect the removal of both of As and BTEX (Yan, et al., 2016; Choi, et al., 2010). Finally, scaling up experimental setting to field applications can also add complications to efficiency and removal rate. There are considerable scaling factor that can contribute to the field significantly but also add errors as indicated in literature (Cheng et al. 2013).

For future work, few areas can be future studied, which are to (1) increase the SiO_2 content ratio in the mixture material to reduce cost of TiO_2; (2) apply engineered TiO_2 under visible light to evaluate BTEX removal (energy reduced mode); (3) employ numerical model to simulate scaling scenarios to assess efficiency and quantify possible errors.

REFERENCES

Adamson, A.W. and Gast, A.P., 1967. Physical chemistry of surfaces (Vol. 15). New York: Interscience.

Aeschbach-Hertig, W. and Gleeson, T., 2012. Regional strategies for the accelerating global problem of groundwater depletion. Nature Geoscience, 5(12), pp.853.

Alizadeh Fard, M., Aminzadeh, B. and Vahidi, H., 2013. Degradation of petroleum aromatic hydrocarbons using TiO2 nanopowder film. Environmental technology, 34(9), pp.1183-1190.

Anderson, C. and Bard, A.J., 1997. Improved photocatalytic activity and characterization of mixed TiO2/SiO2 and TiO2/Al2O3 materials. The Journal of Physical Chemistry B, 101(14), pp.2611-2616.

Anpo, M. and Kamat, P.V. eds., 2010. Environmentally benign photocatalysts: applications of titanium oxide-based materials. Springer Science & Business Media.

Aziz, A. and Kim, K.S., 2017. Synergistic effect of UV pretreated Fe-ZSM-5 catalysts for heterogeneous catalytic complete oxidation of VOC: A technology development for sustainable use. Journal of hazardous materials, 340, pp.351-359.

Bang, S., Patel, M., Lippincott, L. and Meng, X., 2005. Removal of arsenic from groundwater by granular titanium dioxide adsorbent. Chemosphere, 60(3), pp.389-397.

Bang, S., Pena, M.E., Patel, M., Lippincott, L., Meng, X. and Kim, K.W., 2011. Removal of arsenate from water by adsorbents: a comparative case study. Environmental geochemistry and health, 33(1), pp.133-141.

Bharatvaj, J., Preethi, V. and Kanmani, S., 2018. Hydrogen production from sulphide wastewater using Ce3+–TiO2 photocatalysis. International Journal of Hydrogen Energy, 43(8), pp.3935-3945.

Choi, H., Al-Abed, S.R., Dionysiou, D.D., Stathatos, E. and Lianos, P., 2010. TiO2-based advanced oxidation nanotechnologies for water purification and reuse. Sustainability science and engineering, 2, pp.229-254.

Ciesielczuk, T., Rosik-Dulewska, C. and Poluszyńska, J., 2019. The Possibilities of Using Broadleaf Cattail Seeds (Typha latifolia L.) as Super Absorbents for Removing Aromatic Hydrocarbons (BTEX) from an Aqueous Solution. Water, Air, & Soil Pollution, 230(1), p.6.

Costa, A.S., Romão, L.P.C., Araújo, B.R., Lucas, S.C.O., Maciel, S.T.A., Wisniewski Jr, A. and Alexandre, M.D.R., 2012. Environmental strategies to remove volatile aromatic fractions (BTEX) from petroleum industry wastewater using biomass. Bioresource Technology, 105, pp.31-39.

Crawford, R.L. and Crawford, D.L. eds., 2005. Bioremediation: principles and applications (Vol. 6). Cambridge University Press.

Crini, G. and Lichtfouse, E., 2018. Advantages and disadvantages of techniques used for wastewater treatment. Environmental Chemistry Letters, pp.1-11.

Cunningham, J.A., Rahme, H., Hopkins, G.D., Lebron, C. and Reinhard, M., 2001. Enhanced in situ bioremediation of BTEX-contaminated groundwater by combined injection of nitrate and sulfate. Environmental science & technology, 35(8), pp.1663-1670.

Evanko, C.R. and Dzombak, D.A., 1997. Remediation of metals-contaminated soils and groundwater. Ground-water remediation technologies analysis center.

Fitts, C.R., 2002. Groundwater science. Elsevier.

Gleick, P.H., 1993. Water and conflict: Fresh water resources and international security. International security, 18(1), pp.79-112.

Guan, X., Du, J., Meng, X., Sun, Y., Sun, B. and Hu, Q., 2012. Application of titanium dioxide in arsenic removal from water: a review. Journal of Hazardous materials, 215, pp.1-16.

Gupta, S.K. and Chen, K.Y., 1978. Arsenic removal by adsorption. Journal (Water Pollution Control Federation), pp.493-506.

Han, F., Kambala, V.S.R., Srinivasan, M., Rajarathnam, D. and Naidu, R., 2009. Tailored titanium dioxide photocatalysts for the degradation of organic dyes in wastewater treatment: a review. Applied Catalysis A: General, 359(1-2), pp.25-40.

Hering, J.G., Chen, P.Y., Wilkie, J.A., Elimelech, M. and Liang, S., 1996. Arsenic removal by ferric chloride. Journal-American Water Works Association, 88(4), pp.155-167.

Hlihor, R.M., Apostol, L.C. and Gavrilescu, M., 2017. Environmental bioremediation by biosorption and bioaccumulation: principles and applications. In Enhancing Cleanup of Environmental Pollutants (pp. 289-315). Springer, Cham.

Jegadeesan, G., Al-Abed, S.R., Sundaram, V., Choi, H., Scheckel, K.G. and Dionysiou, D.D., 2010. Arsenic sorption on TiO2 nanoparticles: Size and crystallinity effects. Water Research, 44(3), pp.965-973.

Jézéquel, H. and Chu, K.H., 2005. Enhanced adsorption of arsenate on titanium dioxide using Ca and Mg ions. Environmental Chemistry Letters, 3(3), pp.132-135.

Kanel, S.R., Manning, B., Charlet, L. and Choi, H., 2005. Removal of arsenic (III) from groundwater by nanoscale zero-valent iron. Environmental science & technology, 39(5), pp.1291-1298.

Kartinen Jr, E.O. and Martin, C.J., 1995. An overview of arsenic removal processes. Desalination, 103(1-2), pp.79-88.

Katsoyiannis, I.A. and Zouboulis, A.I., 2002. Removal of arsenic from contaminated water sources by sorption onto iron-oxide-coated polymeric materials. Water research, 36(20), pp.5141-5155.

Khodaei, K., Nassery, H.R., Asadi, M.M., Mohammadzadeh, H. and Mahmoodlu, M.G., 2017. BTEX biodegradation in contaminated groundwater using a novel strain (Pseudomonas sp. BTEX-30). International Biodeterioration & Biodegradation, 116, pp.234-242.

Kim, Y., Kim, C., Choi, I., Rengaraj, S. and Yi, J., 2004. Arsenic removal using mesoporous alumina prepared via a templating method. Environmental science & technology, 38(3), pp.924-931.

Leal, J.H., Cantu, Y., Gonzalez, D.F. and Parsons, J.G., 2017. Brookite and anatase nanomaterial polymorphs of TiO2 synthesized from TiCl3. Inorganic Chemistry Communications, 84, pp.28-32.

Li, F.B., Li, X.Z., Ao, C.H., Lee, S.C. and Hou, M.F., 2005. Enhanced photocatalytic degradation of VOCs using Ln^{3+}–TiO_2 catalysts for indoor air purification. Chemosphere, 59(6), pp.787-800.

Li, G.S., Zhang, D.Q. and Yu, J.C., 2009. A new visible-light photocatalyst: CdS quantum dots embedded mesoporous TiO_2. Environmental science & technology, 43(18), pp.7079-7085.

Lu, C., Su, F. and Hu, S., 2008. Surface modification of carbon nanotubes for enhancing BTEX adsorption from aqueous solutions. Applied Surface Science, 254(21), pp.7035-7041.

Ma, L. and Tu, S.X., 2011. Removal of arsenic from aqueous solution by two types of nano TiO 2 crystals. Environmental chemistry letters, 9(4), pp.465-472.

Mao, F., Gaunt, J.A., Cheng, C.L. and Ong, S.K., 2010. Permeation of BTEX compounds through HDPE pipes under simulated field conditions. Journal-American Water Works Association, 102(3), pp.107-118.

Mao, Y., Kanungo, M., Hemraj-Benny, T. and Wong, S.S., 2006. Synthesis and growth mechanism of titanate and titania one-dimensional nanostructures self-assembled into hollow micrometer-scale spherical aggregates. The Journal of Physical Chemistry B, 110(2), pp.702-710.

Mohan, D. and Pittman Jr, C.U., 2007. Arsenic removal from water/wastewater using adsorbents—a critical review. Journal of hazardous materials, 142(1-2), pp.1-53.

Mulligan, C.N., Yong, R.N. and Gibbs, B.F., 2001. Remediation technologies for metal-contaminated soils and groundwater: an evaluation. *Engineering geology*, *60*(1-4),

National Research Council, 1977. Medical and biologic effects of environmental pollutants, arsenic. National Academy of Sciences, Washington, DC, p.219.

Nordstrom, D.K., 2002. Worldwide occurrences of arsenic in ground water.

Oki, T. and Kanae, S., 2006. Global hydrological cycles and world water resources. science, 313(5790), pp.1068-1072.

Paixão, J.F.D., Nascimento, I.A., Pereira, S.A., Leite, M.B.L., Carvalho, G.C.D., Silveira Jr, J.S.C., Rebouças, M., Matias, G.R.A. and Rodrigues, I.L.P., 2007. Estimating the gasoline components and formulations toxicity to microalgae (Tetraselmis chuii) and oyster (Crassostrea rhizophorae) embryos: an approach to minimize environmental pollution risk. Environmental Research, 103(3), pp.365-374.

Peerakiatkhajorn, P., Chawengkijwanich, C., Onreabroy, W. and Chiarakorn, S., 2012. Novel

photocatalytic Ag/TiO2 thin film on polyvinyl chloride for gaseous BTEX treatment. In Materials Science Forum (Vol. 712, pp. 133-145). Trans Tech Publications.

Pena, M., Meng, X., Korfiatis, G.P. and Jing, C., 2006. Adsorption mechanism of arsenic on nanocrystalline titanium dioxide. Environmental Science & Technology, 40(4), pp.1257-1262.

Pena, M.E., Korfiatis, G.P., Patel, M., Lippincott, L. and Meng, X., 2005. Adsorption of As (V) and As (III) by nanocrystalline titanium dioxide. Water Research, 39(11), pp.2327-2337.

Pierce, M.L. and Moore, C.B., 1982. Adsorption of arsenite and arsenate on amorphous iron hydroxide. Water Research, 16(7), pp.1247-1253.

pp.193-207.

Ranck, J.M., Bowman, R.S., Weeber, J.L., Katz, L.E. and Sullivan, E.J., 2005. BTEX removal from produced water using surfactant-modified zeolite. Journal of Environmental Engineering, 131(3), pp.434-442.

Reinhard, M., Hopkins, G.D., Steinle-Darling, E. and LeBron, C.A., 2005. In situ biotransformation of BTEX compounds under methanogenic conditions. Groundwater Monitoring & Remediation, 25(4), pp.50-59.

Schreiber, M.E. and Bahr, J.M., 2002. Nitrate-enhanced bioremediation of BTEX-contaminated groundwater: parameter estimation from natural-gradient tracer experiments. Journal of Contaminant Hydrology, 55(1-2), pp.29-56.

Simantiraki, F. and Gidarakos, E., 2015. Comparative assessment of compost and zeolite utilisation for the simultaneous removal of BTEX, Cd and Zn from the aqueous phase: batch and continuous flow study. Journal of environmental management, 159, pp.218-226.

Smedley, P.L. and Kinniburgh, D.G., 2002. A review of the source, behaviour and distribution of arsenic in natural waters. Applied geochemistry, 17(5), pp.517-568.

Su, F., Lu, C. and Hu, S., 2010. Adsorption of benzene, toluene, ethylbenzene and p-xylene by NaOCl-oxidized carbon nanotubes. Colloids and Surfaces A: Physicochemical and Engineering Aspects, 353(1), pp.83-91.

Su, R., Bechstein, R., Sø, L., Vang, R.T., Sillassen, M., Esbjornsson, B., Palmqvist, A. and Besenbacher, F., 2011. How the anatase-to-rutile ratio influences the photoreactivity of

TiO2. The journal of physical chemistry C, 115(49), pp.24287-24292.

Thamaphat, K., Limsuwan, P. and Ngotawornchai, B., 2008. Phase characterization of TiO2 powder by XRD and TEM. Kasetsart J.(Nat. Sci.), 42(5), pp.357-361.

UNESCO, 2018. United Nations World Water Assessment Programme, 2018. The United Nations World Water Development Report 2018: Nature-Based Solutions for Water, pp154.

US EPA, 2001. National Primary Drinking Water Regulations: Arsenic and Clarifications to Compliance and New Source Contaminants Monitoring. Federal Register, 66 (2001), pp 69-76.

WHO, 1998. Guidelines for drinking-water quality. Vol. 2, Health criteria and other supporting information: addendum (No. WHO/EOS/98.1). Geneva: World Health Organization.

Xu, Z. and Meng, X., 2009. Size effects of nanocrystalline TiO2 on As (V) and As (III) adsorption and As (III) photooxidation. Journal of hazardous materials, 168(2-3), pp.747-752.

Xue, Y., Lu, S., Fu, X., Sharma, V.K., Mendoza-Sanchez, I., Qiu, Z. and Sui, Q., 2018. Simultaneous removal of benzene, toluene, ethylbenzene and xylene (BTEX) by CaO2 based Fenton system: Enhanced degradation by chelating agents. Chemical Engineering Journal, 331, pp.255-264.

Yan, L., Hu, S. and Jing, C., 2016. Recent progress of arsenic adsorption on TiO2 in the presence of coexisting ions: A review. Journal of Environmental Sciences, 49, pp.74-85.

Zalel, A. and Broday, D.M., 2008. Revealing source signatures in ambient BTEX concentrations. Environmental pollution, 156(2), pp.553-562.

Zou, L., Luo, Y., Hooper, M. and Hu, E., 2006. Removal of VOCs by photocatalysis process using adsorption enhanced TiO2–SiO2 catalyst. Chemical Engineering and Processing: Process Intensification, 45(11), pp.959-964.

Zytner, R.G., 1994. Sorption of benzene, toluene, ethylbenzene and xylenes to various media. Journal of hazardous materials, 38(1), pp.113-126.

APPENDIX A

APPENDIX A

TABLES

Table 1. Treatment technologies for arsenic in groundwater

Technology	Cost	Operability	Removal Effect	Stability for long-term
Subsurface Barriers	low	high	high	high
Solidification	low	high	high	moderate
Vitrification	moderate	high	high	moderate
Biological Treatment	moderate	very high	very high	low
Physical Separation	very high	moderate	very high	high
Pyrometallurgical Extraction	very high	low	very high	high
Electrokinetic Treatment	very high	Low	very high	moderate

Table 2. The maximum contaminant level (MCL) of BTEX

Chemical	MCL(mg/L)
benzene	0.005
toluene	1
ethylbenzene	0.7
xylenes (total)	10

Table 3. Laboratory experimental parameters

Parameter	Value	Unit
Flow rate	0.1-10.0	ml/min
Initial concentration of arsenic	0.15-0.7	mg/L
Initial concentration of gasoline (BTEX)	4.5-10.5	mg/L
pH	7±0.5	
Temperature	25	°C
Pressure	101.325	kPa

Table 4. The characterizations of two nano-TiO_2

	Aggregated dendritic TiO_2	Nano-TiO_2 attached to the SiO_2
Characterizations	Spreading many of these dendritic tentacles on the surface of materials.	The surface of the material is uneven, and there are many spherical and hemispherical bulges.
Form	Anatase	Rutile
Arrangement	There are large holes between the aggregated particles	Material coverage is tight

Table 5. The data of arsenic adsorption efficiency curve

C_0=634ppb					
Aggregated TiO_2	mean	SE	Attached TiO_2	mean	SE
0	0		0	0	
5	0.09858	0.0145	5	0.04259	0.051
10	0.15457	0.065	10	0.18849	0.0785
20	0.37618	0.0115	20	0.42192	0.0005
30	0.63407	0.01	30	0.57965	0.0155
40	0.69322	0.0035	40	0.66009	0.0125
50	0.73896	0.0025	50	0.69322	0.0025
60	0.7295	0.0015	60	0.6877	0.018

C_0=167ppb					
Aggregated TiO_2	mean	SE	Attached TiO_2	mean	SE
0	0		0	0	
5	0.05389	0.002	5	0.12874	0.0015
10	0.07784	0.001	10	0.20359	0.001
20	0.11078	0.0005	20	0.23353	0.002
30	0.27246	0.0015	30	0.23653	0.0005
40	0.30539	0.001	40	0.28743	0.001
50	0.29641	0.0025	50	0.28743	0.001
60	0.29341	0	60	0.2994	0.001

Table 6. The data of Arsenic removal rate

C_0=634ppb					
Aggregated TiO_2	Mean(%)	SE	Attached TiO_2	Mean(%)	SE
0	0		0	0	
1	0.54	0.018	1	0.6	0.02
2	0.65	0.039	2	0.69	0.012
4	0.82	0.026	4	0.79	0.025
6	0.92	0.033	6	0.9	0.04
8	0.93	0.025	8	0.91	0.021
10	0.96	0.040	10	0.92	0.03
12	0.94	0.042	12	0.92	0.028
15	0.95	0.024	15	0.93	0.013

C_0=167ppb					
Aggregated TiO_2	Mean(%)	SE	Attached TiO_2	Mean(%)	SE
0	0		0	0	
1	0.46215	0.019	1	0.48896	0.039
2	0.54259	0.026	2	0.58833	0.025
4	0.66088	0.032	4	0.63249	0.033
6	0.71451	0.044	6	0.72658	0.031
8	0.75237	0.039	8	0.77445	0.043
10	0.78076	0.01	10	0.79653	0.034
12	0.82019	0.009	12	0.8265	0.043
15	0.83523	0.025	15	0.82019	0.031

Table 7. The data of total BTEX degradation efficiencies in different condition

Only UV(C_0=4.25ppm)	Mean(%)	SE
0	1	
10	0.99215	0.00333
20	0.98038	0.00333
30	0.96782	0
40	0.95761	0.00882
50	0.94741	0.00667
60	0.93485	0.00577
70	0.92229	0.00667

Aggregated TiO_2		
UV+TiO_2	Mean(%)	SE
0	1	
10	0.85322	0.01856
20	0.70801	0.01333
30	0.53768	0.01453
40	0.36028	0.00577
50	0.22449	0.01453
60	0.15856	0.02906
70	0.13265	0.01764
UV+TiO_2+H_2O_2	Mean(%)	SE
0	1	
10	0.53925	0.01528
20	0.38619	0.03215
30	0.26688	0.0393
40	0.15934	0.02028
50	0.10518	0.01453
60	0.08477	0.00577
70	0.05573	0.00882

Attached TiO_2		
$UV+TiO_2$	Mean(%)	SE
0	1	
10	0.83516	0.04055
20	0.64678	0.05796
30	0.50157	0.02646
40	0.35479	0.04667
50	0.29827	0.03528
60	0.27786	0.03215
70	0.25432	0.03464
$UV+TiO_2+H_2O_2$	Mean(%)	SE
0	1	
10	0.50157	0.04041
20	0.34223	0.03756
30	0.26609	0.02646
40	0.14129	0.05115
50	0.11617	0.02404
60	0.11381	0.01453
70	0.09105	0.01202

Table 8. The data of total BTEX degradation efficiencies for two TiO_2

Only UV(C_0=10.17ppm)	Mean(%)	SE
0	1	
10	0.99475	0.00333
20	0.99279	0.00333
30	0.98721	0.00882
40	0.9823	0.01202
50	0.97541	0.00882
60	0.97049	0.00333
70	0.96459	0.01202

Aggregated TiO_2		
UV+TiO_2	Mean(%)	SE
0	1	
10	0.89541	0.00667
20	0.77869	0.00882
30	0.6082	0.00882
40	0.42557	0.01202
50	0.29934	0.01202
60	0.2377	0.02333
70	0.21443	0.00577

Attached TiO_2		
UV+TiO_2	Mean(%)	SE
0	1	
10	0.87705	0.02603
20	0.67508	0.02603
30	0.5777	0.02728
40	0.44754	0.01732
50	0.36623	0.01764
60	0.33607	0.02028
70	0.31902	0.02333

APPENDIX B

APPENDIX A

FIGURES

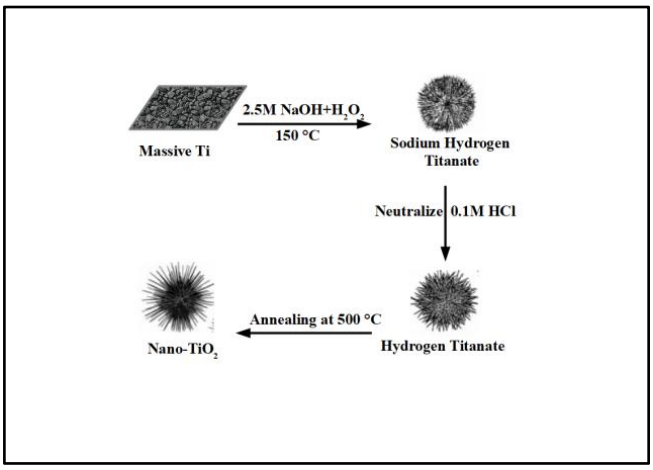

(a)

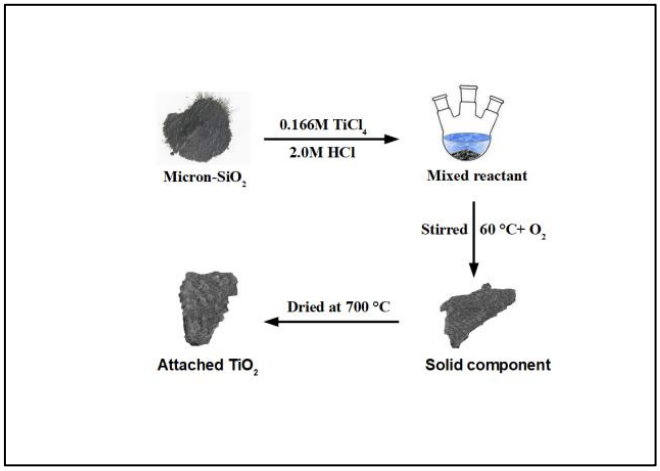

(b)

Figure. 1. Preparation of two kinds of TiO_2 in laboratory. (a)the aggregated dendritic nano-scale TiO_2, (b) nano-TiO_2 attached to the surface of SiO_2

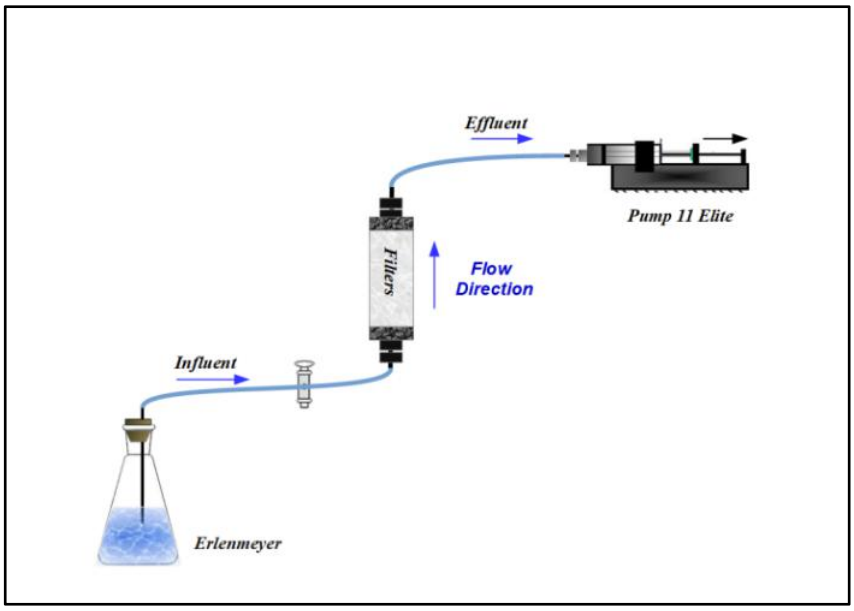

(a)

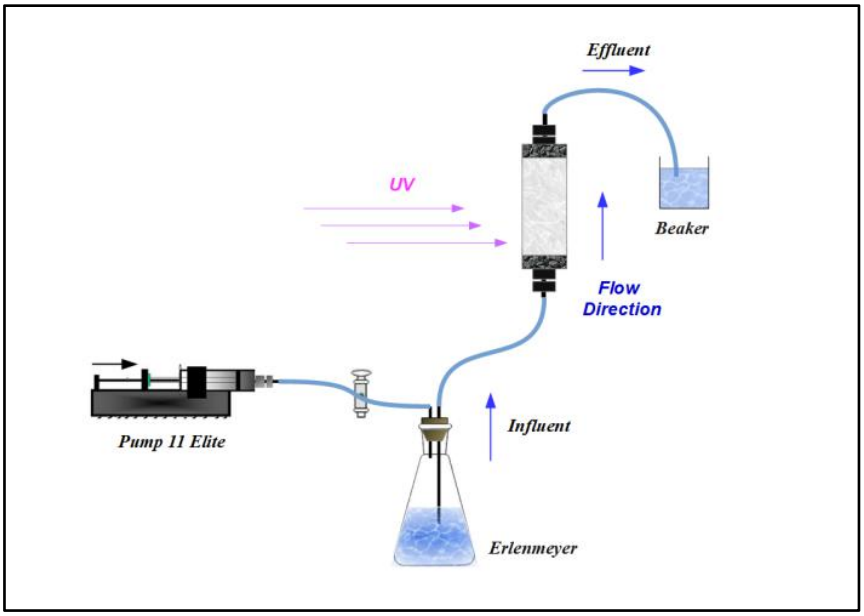

(b)

Figure. 2. Synoptical diagram of the system used in the experiment, including the Erlenmeyer, switch, pump 11 Elite, Column Filters, and Catheter. (a) the experimental design for removing As,, (b) the experimental design for removing BTEX.

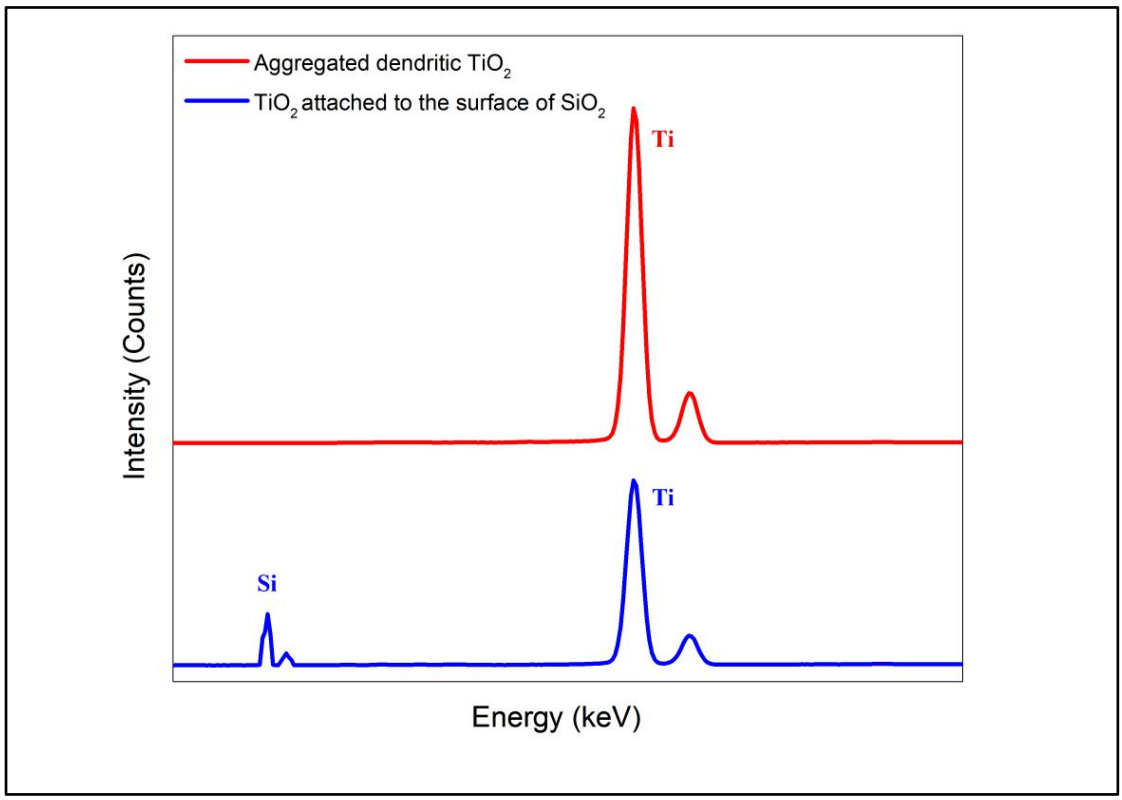

Figure. 3. The XRF of two materials before the experiment. The red curve is aggregated dendritic TiO_2, while the blue curve is TiO_2 attached to the surface of SiO_2.

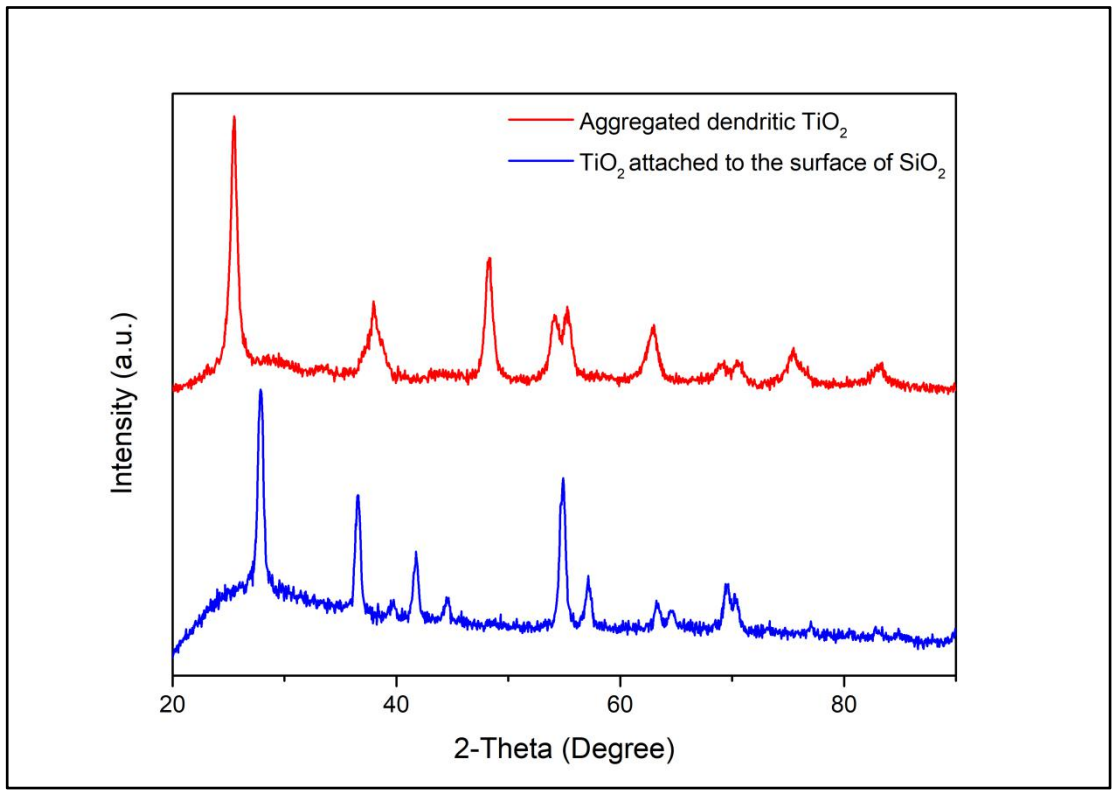

Figure. 4. The XRD pattern of different nono-TiO_2 before the experiment. The red curve means aggregated dendritic TiO_2, and the blue curve is the representative of TiO_2 attached to the surface of SiO_2

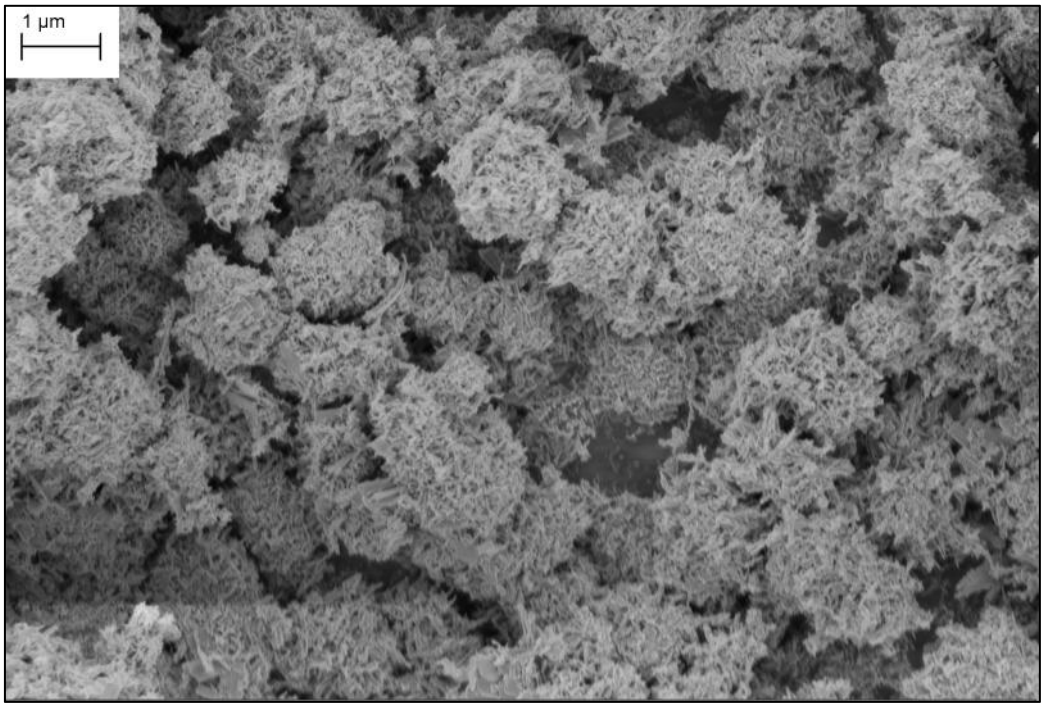

(a)

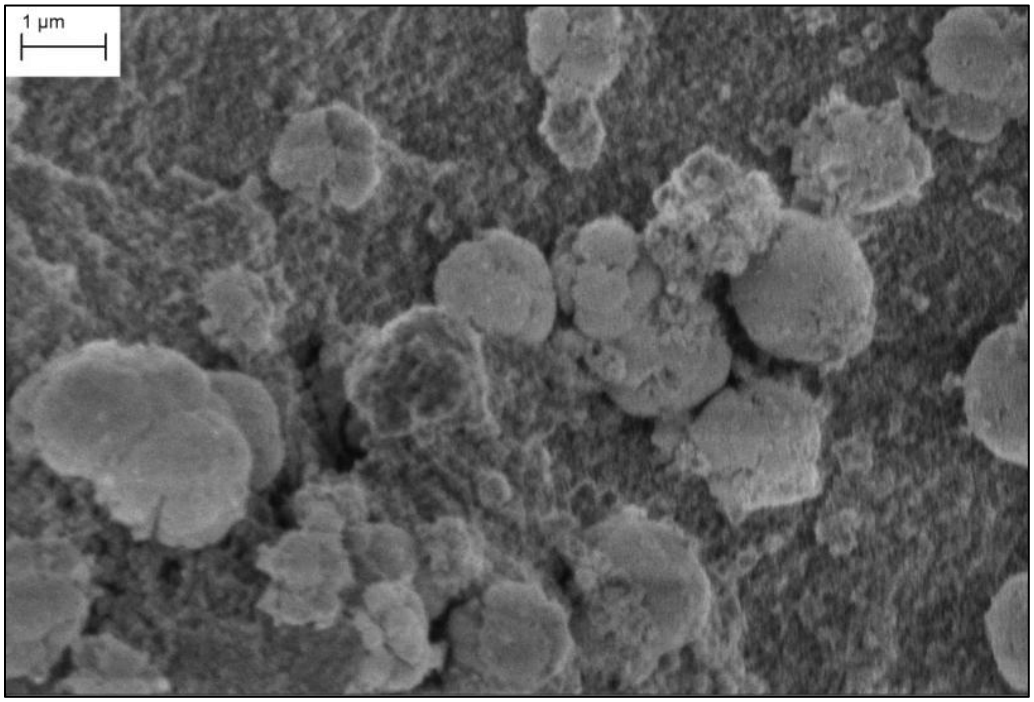

(b)

Figure. 5. Characterization of two nano-TiO_2 observed using SEM. (a) the aggregated dendritic TiO_2, (b) the TiO_2 attached to the surface of SiO_2.

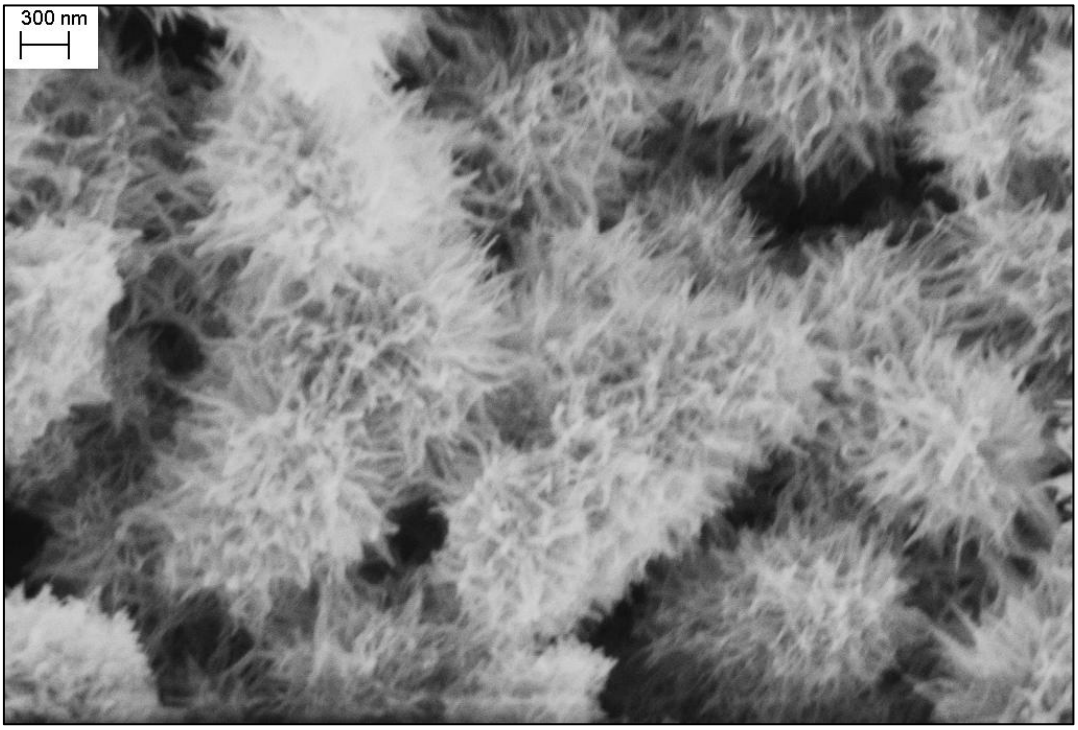

Figure. 6. The SEM characterization of sodium titanate, which was papered for making aggregated dendritic TiO_2.

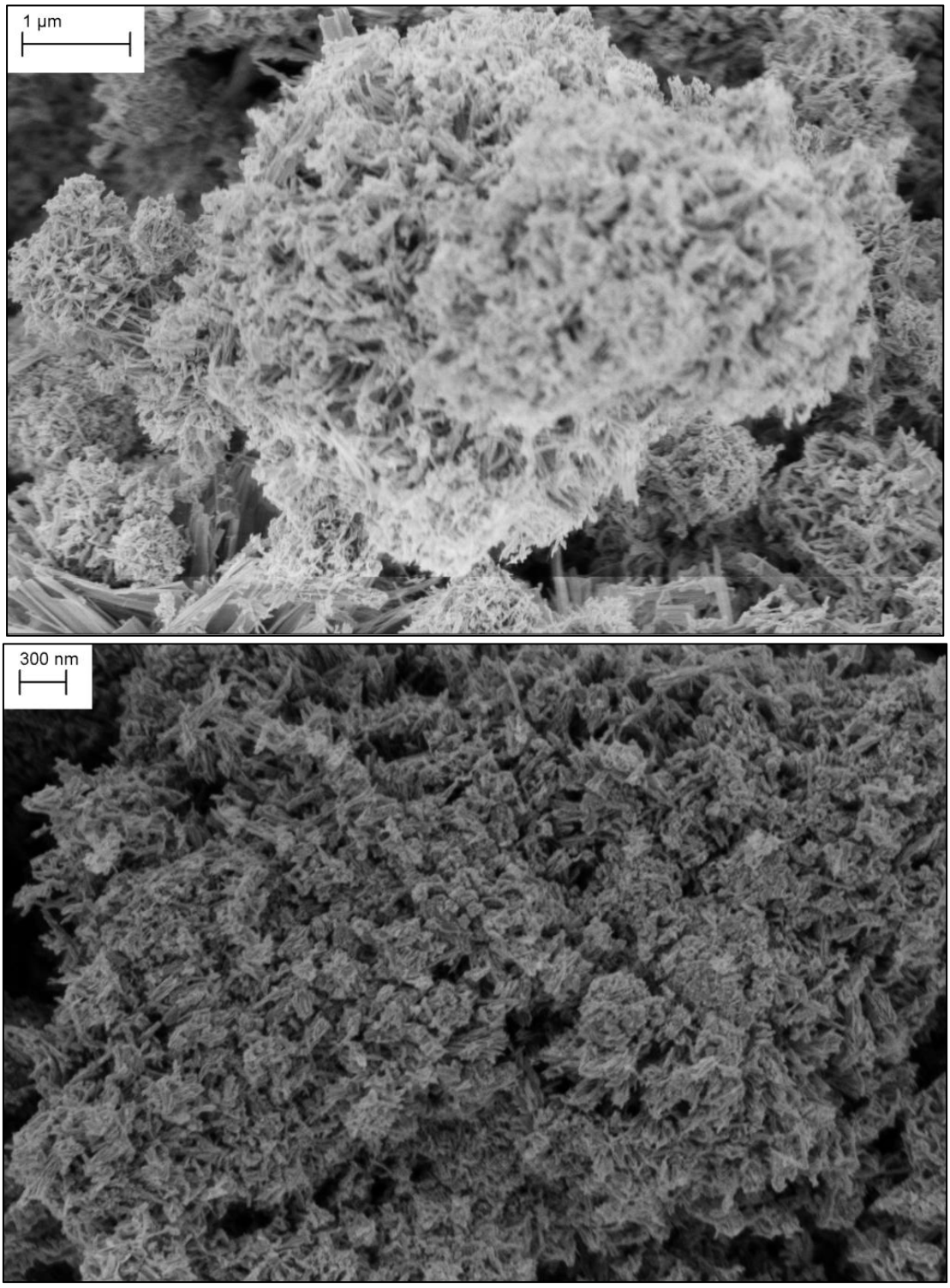

Figure. 7. The SEM observations of aggregated dendritic TiO_2 at different magnifications

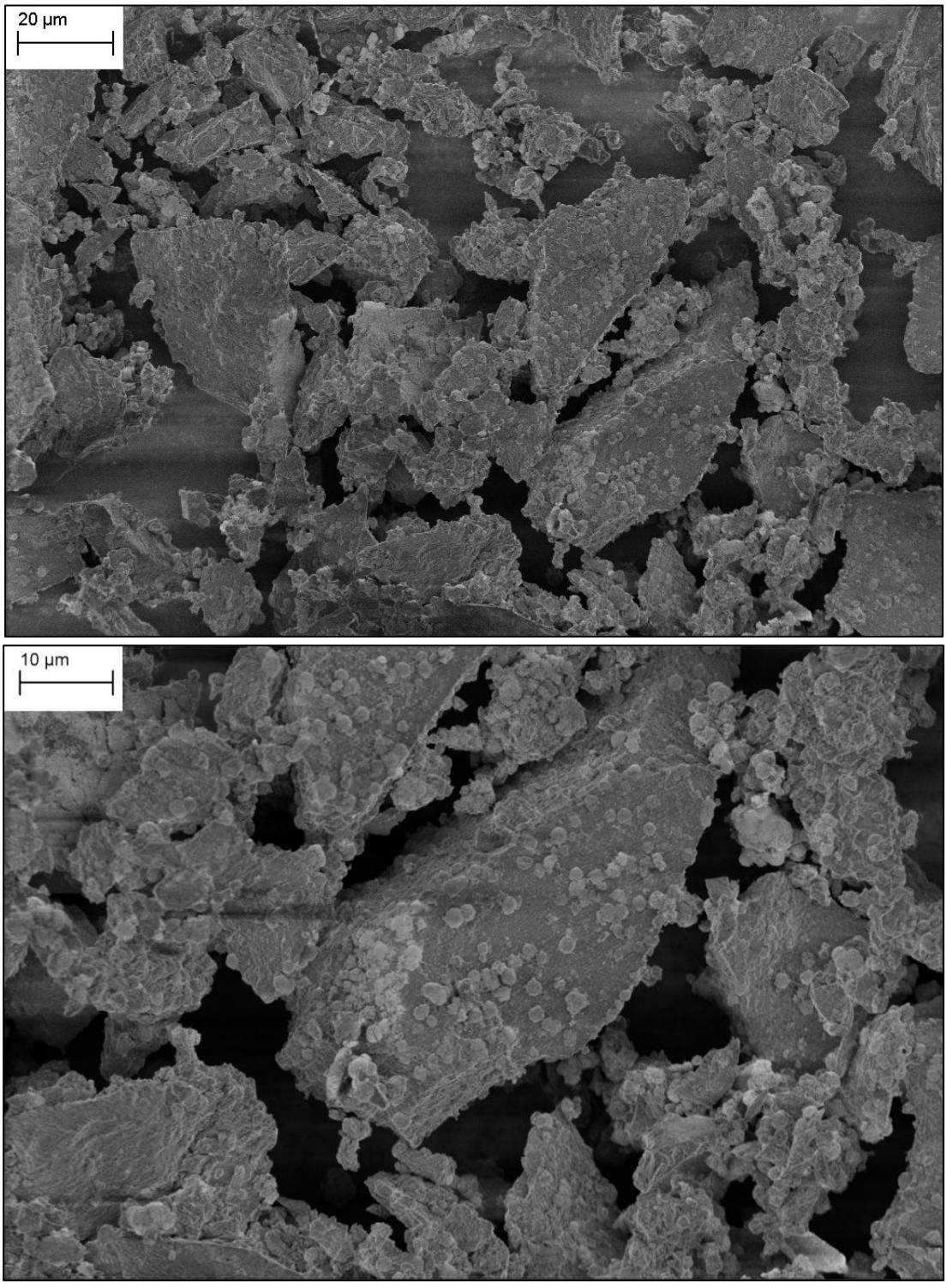

Figure. 8. The SEM observations of TiO_2 which attached to the surface of SiO_2 at different magnifications.

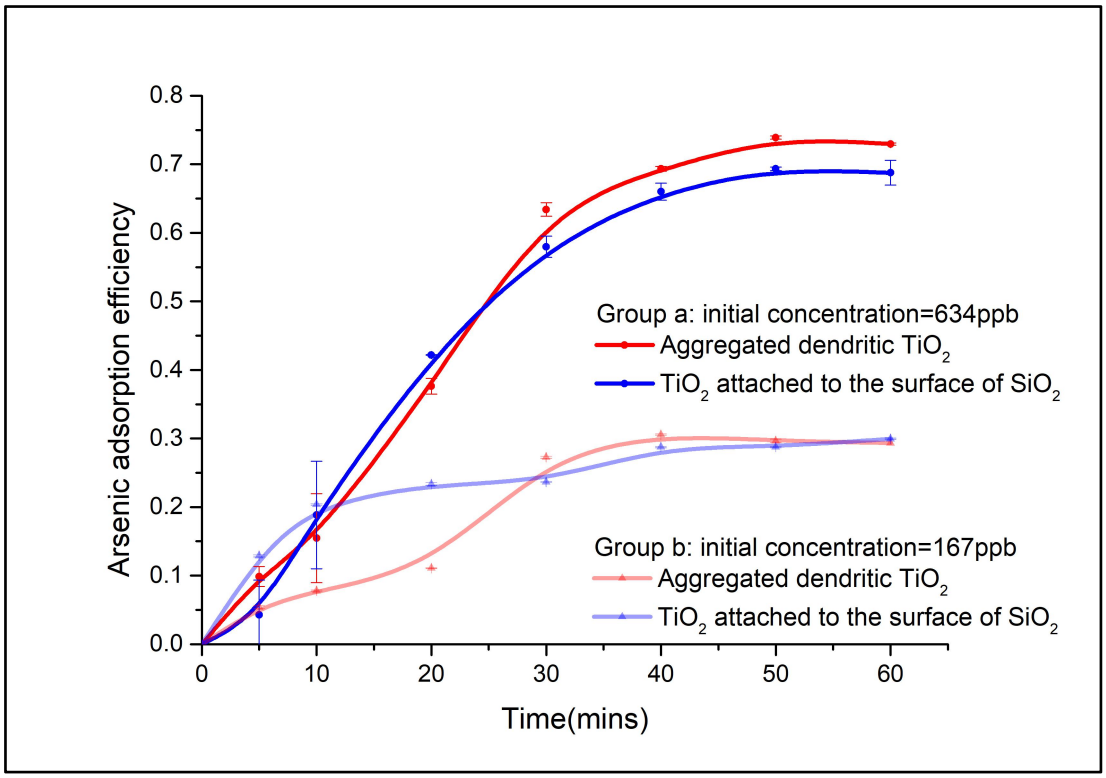

Figure. 9. Adsorption efficiency curve of different arsenic concentrations. The red curve means aggregated dendritic TiO_2, and the blue curve is the representative of TiO_2 attached to the surface of SiO_2. and the Group a and b represent arsenic concentrations of 634ppb and 167ppb, respectively.

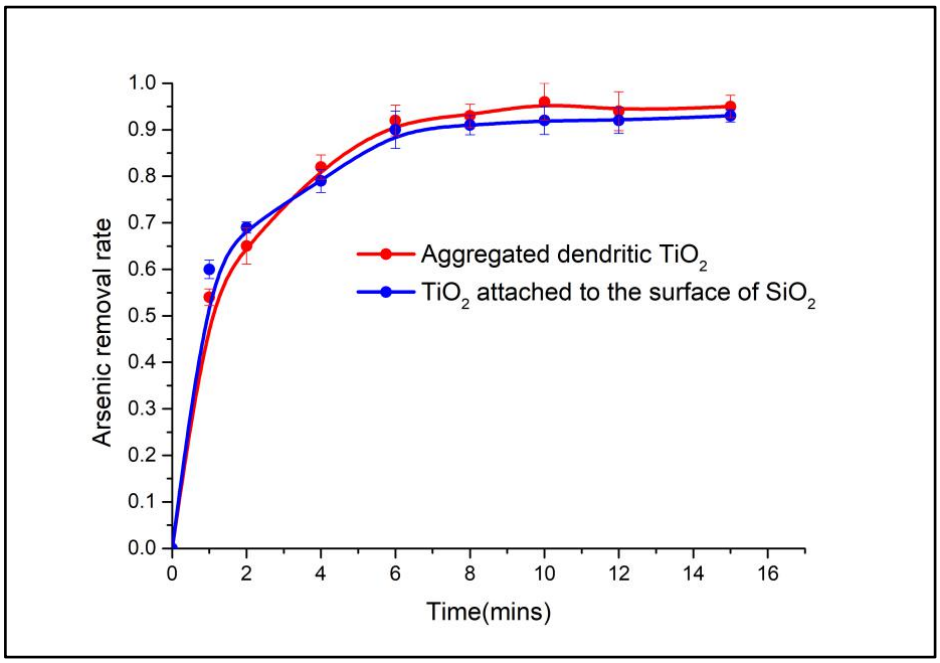

(a)

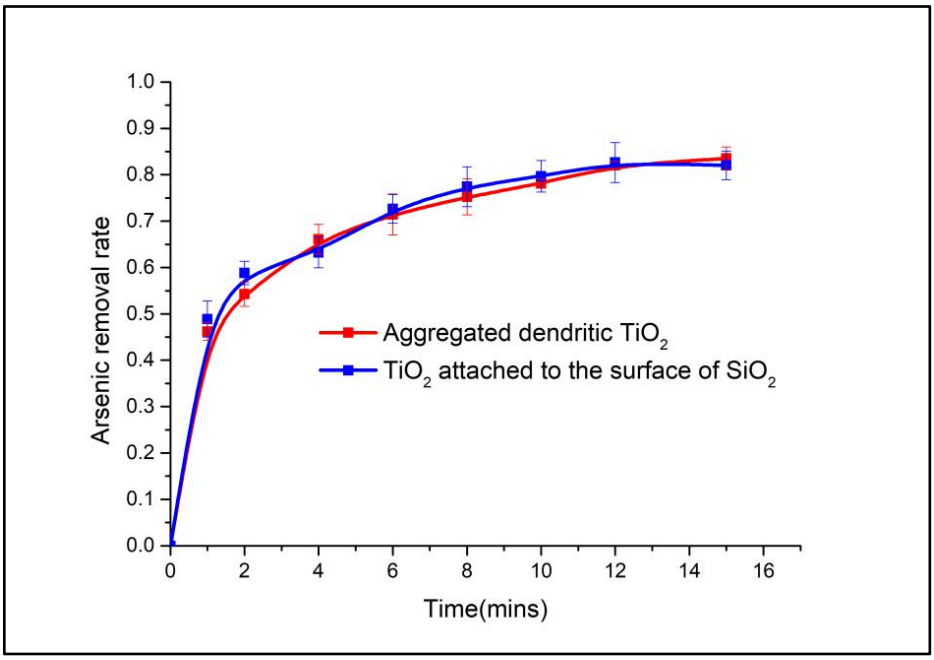

(b)

Figure. 10. Arsenic removal rate on the laboratory injection system. The red curve is aggregated dendritic TiO_2, and the blue curve is TiO_2 attached to the surface of SiO_2. (a) The initial concentration of arsenic solution is 634ppb, and (b) is 167ppb.

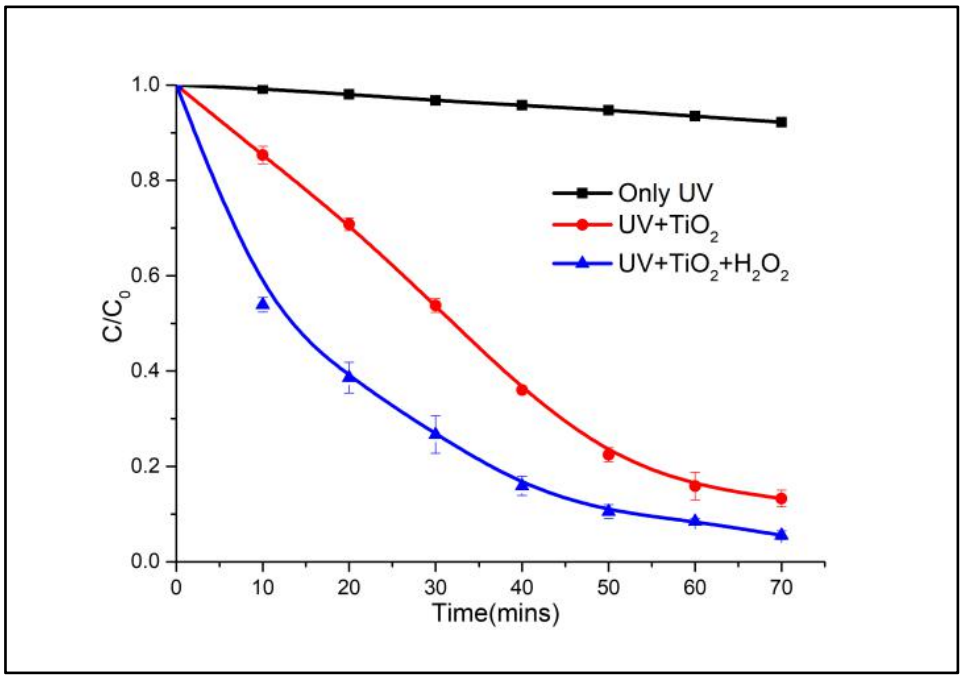

(a)

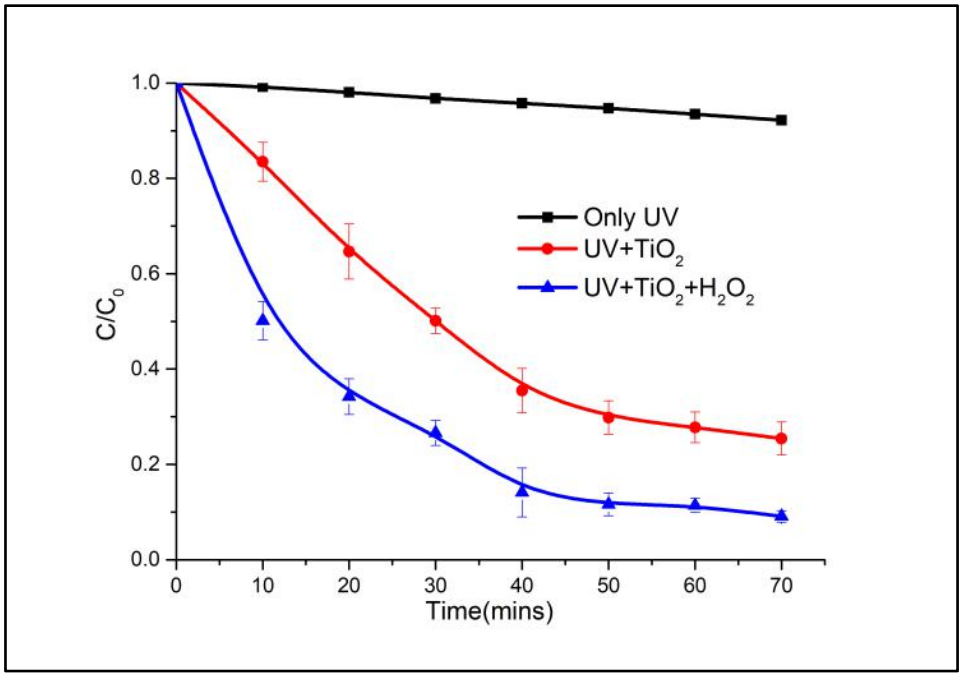

(b)

Figure. 11. The total BTEX degradation efficiencies in three different condition. (a) is aggregated dendritic TiO_2, and (b) is TiO_2 attached to the surface of SiO_2. C_0=4.25ppm

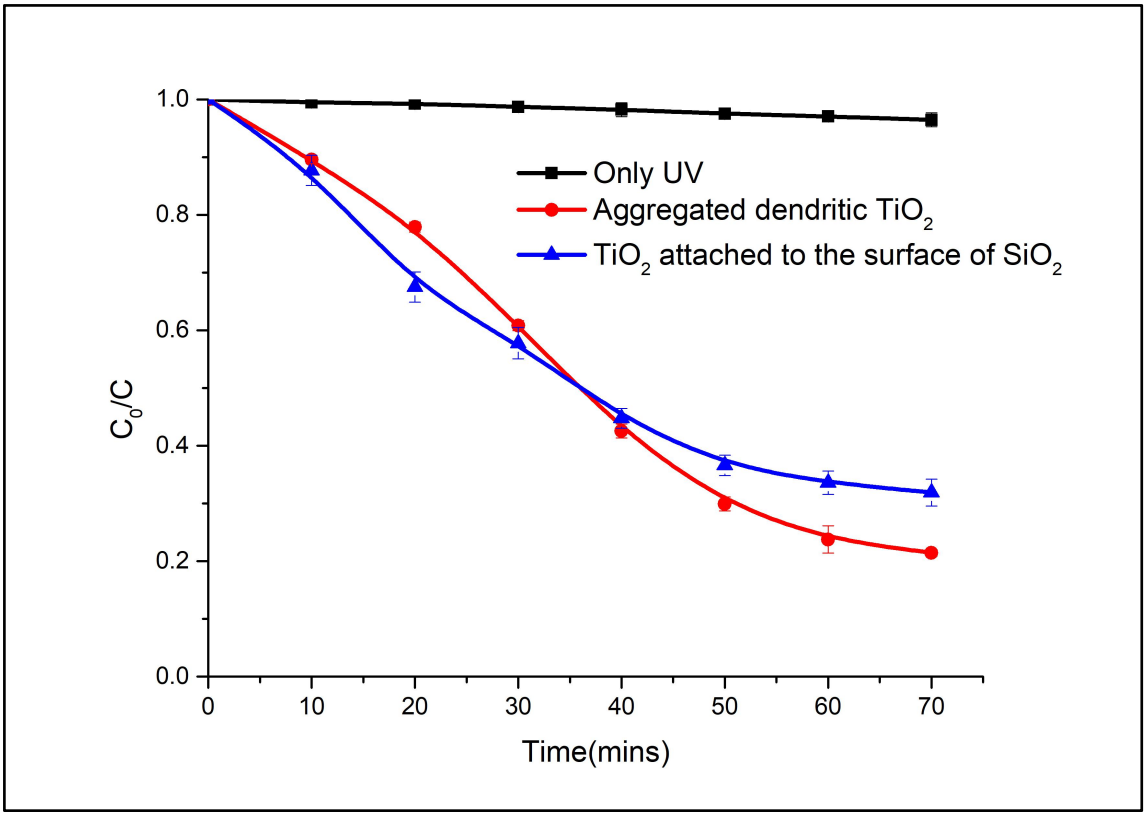

Figure. 12. The removal efficiencies for high total BTEX concentration (C_0=10.17ppm). The red curve is aggregated dendritic TiO_2, while the blue curve means TiO_2 attached to the surface of SiO_2.

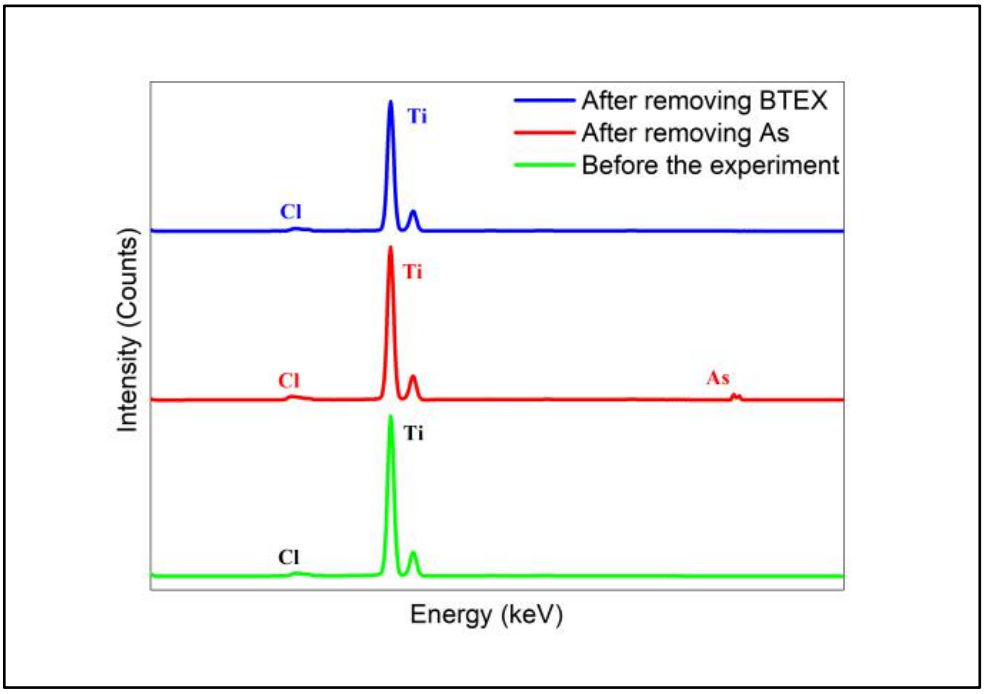

(a)

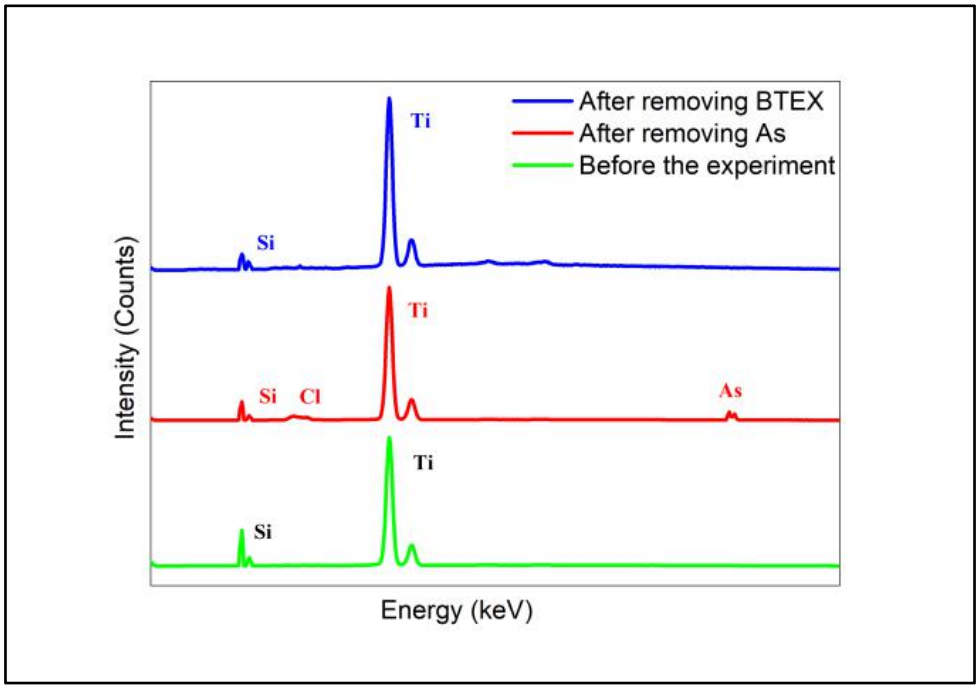

(b)

Figure. 13. XRF diagram before and after the experiment. (a) the XRF of the aggregated dendritic TiO_2, (b) the XRF of TiO_2 attached to the surface of SiO_2.

BIOGRAPHICAL SKETCH

Sheng Yin was born in Wuhan, China in 1994. He received his bachelor's degree in environmental engineering from the Wuhan Institute of Technology in Fall 2016. He earned the master's degree in Agricultural, Environmental, and Sustainability Sciences under School of Earth, Environmental and Marine Sciences from the University of Texas Rio Grande Valley in Summer 2019. He will be pursuing his Ph.D. degree in Environmental Engineering and Science or Environmental Chemistry in Fall 2019 (school TBD). He aims to continue his research in the applications engineered materials for environmental remediation and water treatments.

His personal email is sheng.yin01@utrgv.edu